



Research Article

Heat transfer analysis using a duct filled with metal foams

Abhisek BANERJEE¹, Diplina PAUL²

¹Intel Corporation, Chandler, AZ, USA, 85248

²Department of Biological and Agricultural Engineering, North Carolina State University, Raleigh, NC USA 27607

ARTICLE INFO

Article history

Received: 07 September 2020

Accepted: 28 January 2021

Keywords:

Conjugate Heat Transfer; Heat Pipes; Heat Exchangers; Porous Media; Reynolds Number; Nusselt Number

ABSTRACT

Thick-walled pipe experiencing internal flow is widely used in a variety of applications in the industry. Some of the most prominent ones are heat exchangers, heat pipes, furnaces, etc. In this study, conjugate heat transfer has been examined in a pipe filled with a porous medium experiencing a constant external heat flux. The analysis is based on a two-dimensional domain using a quasi-thermal equilibrium model. Effects of porosity, pore density, Reynold's number and thermal conductivity of solid and fluid on the Nusselt number have been studied. Three types of porous foams based on the pore density have been chosen for the analysis: 10 PPI, 40 PPI and 60 PPI. The results have been generalized for use in a wide range of Newtonian fluids. Additionally, the pressure drops across the pipes filled with porous media have been studied as a function of pore density and Reynold's number. Numerical results indicate augmented performance with porous foams of high pore densities. However, using a porous medium with higher pore density leads to higher pressure drop, thus needing pumping power. The computational model used in this manuscript predicts that Nusselt number is increased by 38.7 % with Reynold's number < 10000, when the porous medium is changed from 10 PPI to 60 PPI. The numerical data presented in the manuscript supports the application of low porosity foam with low pore density to achieve better thermal transport at the cost of pressure drop.

Cite this article as: Banerjee A, Paul A. Heat transfer analysis using a duct filled with metal foams. J Ther Eng 2022;8(4):529–537.

INTRODUCTION

Last few decades have witnessed a wide range of applications for high porosity metal foams in various forms of structures like aircraft wings, catalytic surfaces for chemical reactions, structural elements to support high stress, combustion systems to burn solid fuels, cooling of nuclear reactors, heat exchangers and may others. High surface-area

density, light weight, high thermal conductivity and excellent mixing capability for the fluid, open cell foams have been greatly studied for heat exchangers.

The understanding of various thermal transport phenomena is a very significant aspect of utilizing porous foams for heat exchanger related applications. At the very

*Corresponding author.

*E-mail address: abhisekiitg@gmail.com

This paper was recommended for publication in revised form by Regional editor Jovana Radulovic



outset, Darcy addressed the complex fluid flow correlations in porous medium in the year 1856. This law (Darcy's law) however neglects the viscous forces acting on the impermeable solid boundary. To comprehend the disadvantages, Brinkman extended Darcy's model to include the effect of viscous forces on solid non-permeable boundary [1]. Few years later, Whitaker [2] and Fand [3] modified Darcy's correlations for use in high Reynold's number flows. In 1988, Calimadi [4] was one of the first researchers to study transport phenomenon in porous medium using these correlations to model energy transport without local thermal equilibrium. He postulated correlations for thermal dispersion conductivity and the interstitial heat transfer coefficient for the first time.

Around the same time, researchers had started to investigate experimental [5-7] and numerical aspects of conjugate heat transfer in pipe flow. Lin and Kuo [6] studied unsteady forced convective heat transfer as a function of Peclet number, radius ratio, conductivity ratio etc. and reported wall-to-fluid heat capacity ratio as the decisive parameter in the thermal transport mechanism. In 2000, Kim et al. [8] studied porous medium as a combination of microchannels and presented analytical solution for their temperature distribution. They also reported the error map which is helpful to identify the applicability of one-equation thermal transport model in practical engineering problems. On the frontier of numerical modelling, Boomsma and Paulikakos [9] contributed significantly by studying the numerical model using 3-D open cell geometry to verify the significance of treating solid and fluid phase temperature distinctly. They reported the dominance of solid thermal conductivity towards effective thermal conductivity in case of high porosity foams. A year later, Bhattacharya et al. [10] reported a detailed analysis of the thermophysical properties like permeability, effective thermal conductivity etc. for high porosity open cell foams. They developed a permeability model based on porosity, pore diameter and tortuosity of metal foams. Nazar et al. [11] used Brinkman model to study mixed convection in porous medium. They reported that the change in the solid-state temperature is significant to impact boundary layer separation and this separation could be delayed using higher solid-state temperature.

Around the same time, Zhao and co-researchers [12-14] followed the same route as Nazar et al. [11] and used Brinkman model to study thermal analysis on metal foam filled heat exchangers. They presented that the pore size and porosity of metal foams play a significant role in governing overall heat transfer coefficient. Extending the work of Zhao et al. [13] this investigation has been conducted to implement Brinkman-extended Darcy model in momentum equation for analyzing the velocity distribution in the metal-foam filled ducts. In 2008, Mahjoob and Vafai [15] developed a model for fluid and thermal transport for metal foam heat exchangers. They quantified a 15 % gain in the thermal transport when porous inserts were used in the

heat exchangers. A year later, DeGroot et al. [16] undertook a numerical study to investigate the details of forced convection in aluminum foam heat sinks and supported that solid to fluid thermal conductivity ratios and Peclet number of the flowing fluid play a significant role in describing the temperature profiles of the solid and fluid region of the tested domain.

Last decade has witnessed a great development in the domain of porous medium. On one side as there are researchers investigating the solid-fluid inter-phasic interaction for various regimes of flow through porous medium [17,18], there are many researchers [19-27] investigating the scope and implementation of porous medium towards applications involving thermal transport. As mentioned above, there is a plethora of research available that supports the advantages of using porous foam to augment thermal transport. Even though one can find a good amount of literature which defines the modeling strategies of porous foams in heat exchangers, authors feel that there is a need to study the governing parameters like porosity, ratio of thermal conductivity of fluid to solid, pressure drop etc, which impact thermal transport through porous medium significantly. To the best of the knowledge of the authors, for first time researchers have attempted to study the impact of parameters like pore density, porosity, Reynolds number and pressure drop on the Nusselt number. This analysis is useful for industrial applications like heat exchangers, heat pipe, furnaces etc.

COMPUTATIONAL MODEL

The computational model has been represented in Fig.1. The entire analysis has been performed on the basis of non-dimensional parameters to eliminate the variation of the geometrical design of the system. 2D numerical simulation has been performed in Fluent 6.4 using a quasi-thermal equilibrium model. The fluid temperature at inlet has been taken as 273 K. The computational investigation has been performed under assumptions such as (i) thermal properties of reactants and products are functions of temperature and concentration only, (ii) the porous medium has homogenous porosity and is chemically inert,

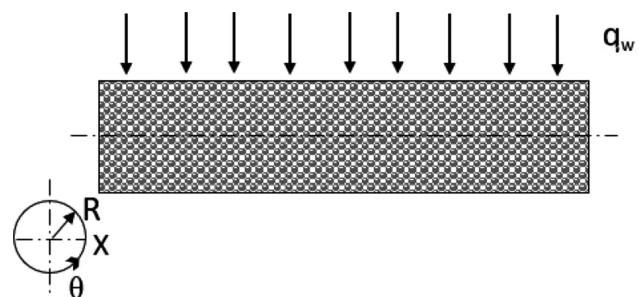


Figure 1. The computational model of the study.

(iii) the solid and fluid phases exist in quasi-thermal non-equilibrium inside the pipe. The computational model has been simulated assuming that the duct is homogeneously filled with the porous foams of 10 PPI, 40 PPI and 60 PPI, where PPI stands for pores per inch. 10 PPI, 40 PPI and 60 PPI foams have 10, 40 and 60 pores per inch length of the foam, respectively. The foams studied here are rectangular in structure (since the simulation is 2-D) with dimension 10 mm × 4 mm. The foams studied here are considered to chemically inert and homogeneously distributed across the radial and axial length of the duct.

MATHEMATICAL FORMULATION

The computational flow field is assumed to be symmetric with respect to the pipe axis. The set of governing equations [19] applicable for the domain is as follows:

Continuity equation

$$\frac{\partial(\rho_f u)}{\partial x} + \frac{1}{r} \frac{\partial(\rho_f v r)}{\partial r} = 0 \quad (1)$$

Momentum equation

$$\begin{aligned} \frac{\partial(\rho_f u^2)}{\partial x} + \frac{1}{r} \frac{\partial(\rho_f r u v)}{\partial r} = & -\epsilon^2 \frac{\partial p}{\partial x} + \frac{\partial}{\partial x} \left(\eta_f \epsilon \frac{\partial u}{\partial x} \right) \\ & + \frac{1}{r} \frac{\partial}{\partial r} \left(r \eta_f \epsilon \frac{\partial u}{\partial x} \right) - \frac{\eta_f \epsilon^2}{K} u - \frac{\rho_f \epsilon^2 C u^2}{\sqrt{K}} \end{aligned} \quad (2)$$

$$\begin{aligned} \frac{\partial(\rho_f u v)}{\partial x} + \frac{1}{r} \frac{\partial(\rho_f r v^2)}{\partial r} = & -\epsilon^2 \frac{\partial p}{\partial r} + \frac{\partial}{\partial x} \left(\eta_f \epsilon \frac{\partial v}{\partial x} \right) \\ & + \frac{1}{r} \frac{\partial}{\partial r} \left(r \eta_f \epsilon \frac{\partial v}{\partial x} \right) - \frac{\eta_f \epsilon^2}{K} v - \frac{\rho_f \epsilon^2 C v^2}{\sqrt{K}} \end{aligned} \quad (3)$$

Energy equation

$$\frac{\partial}{\partial x} \left(k_{se} \frac{\partial T_s}{\partial x} \right) + \frac{1}{r} \frac{\partial}{\partial r} \left(r k_{se} \frac{\partial T_s}{\partial r} \right) - h_{sf} a_{sf} (T_s - T_f) = 0 \quad (4)$$

$$\begin{aligned} \frac{\partial(\rho_f u T_f)}{\partial x} + \frac{1}{r} \frac{\partial(r \rho_f v T_f)}{\partial r} = & \frac{\partial}{\partial x} \left(\frac{k_{fe} + k_d}{C} \frac{\partial T_f}{\partial x} \right) \\ & + \frac{1}{r} \frac{\partial}{\partial r} \left(r \frac{k_{fe} + k_d}{C} \frac{\partial T_f}{\partial r} \right) + \frac{h_{sf} a_{sf}}{C} (T_s - T_f) \end{aligned} \quad (5)$$

The tortuosity of metal foams enhances the coefficients of heat transfer between solid matrix and fluid. The coefficients k_{fe} , k_{se} , k_d , h_{sf} and a_{sf} are calculated using the relationships established by Zhao et al. [12]. At the solid-fluid interface, the two-equation model cannot be used directly since the wall is impermeable to the fluid. At the interface, the dispersion conductivity is considered zero with infinite fluid viscosity producing null fluid velocity. This results in

the equivalence of temperature and efficient thermal conductivity of the solid and fluid. Thus, at the interface the energy equation is reduced to as follows:

$$\frac{\partial}{\partial x} \left(k_{se} \frac{\partial T_s}{\partial x} \right) + \frac{1}{r} \frac{\partial}{\partial r} \left(r k_{se} \frac{\partial T_s}{\partial r} \right) = 0 \quad (6)$$

The boundary conditions specified for this problem are:

- a. The computational model is simulated to have no radial variation of velocity.
 - b. The wall of the pipe is having a no-slip boundary condition.
 - c. The flow is laminar.
 - d. The outer surface of the pipe is heated with constant heat flux.
 - e. At inlet: $v_{in} = 0.3 \frac{m}{s}$; $T_{in} = 298K$
 - f. At outlet: $P_o = P_{atm}$
- The boundary conditions imposed on the solid domain are:

- a. At the outer wall of the solid

$$@r = r_o, 0 \leq x \leq L, q = k_s \frac{\partial T}{\partial r}$$

- b. At the inner wall of the solid

$$T_s = T_f$$

GRID INDEPENDENCE STUDY

The flow field has been meshed using structured rectangular grids (Fig. 2a). A grid independence study has been performed to optimize the number and size of the grids for the present model (Fig. 2b). In this case 125000 grids were chosen to conduct the simulation. The staggered grid arrangement provides the estimation of the pressure using the SIMPLE algorithm by successively predicting and correcting velocity components and pressure. The momentum and energy equations have been discretized using the second-order upwind scheme. The convergence criteria for continuity, momentum and energy equation was set at 10^{-6} . The under-relaxation parameters for pressure, density, bod forces and momentum is set as 0.3, 1, 1 and 0.7 respectively. For this manuscript pressure drop and Nusselt number have been calculated using custom field function in Fluent 6.4 [28, 29]. Fluent calculates the pressure and temperature difference between two cells on their average temperature and then integrates them over the entire computational surface.

MODEL VALIDATION

The numerical model used to study various aspects of the conjugate heat transfer in a pipe filled with a porous medium has been validated against the data published by Du et al. [30]. Du et al. [30] have studied the heat transfer in a 2D pipe with dimensions 200 × 8 mm. For model

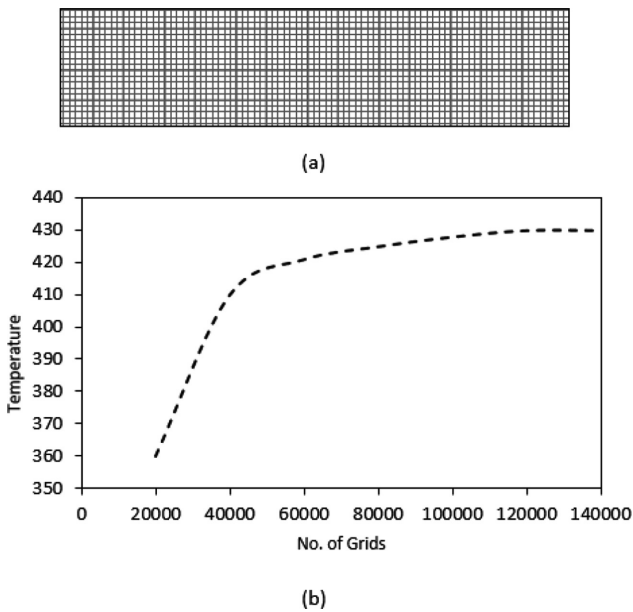


Figure 2. (a) Meshing of the computational domain; (b) grid independence study: variation of temperature with number of grids.

verification, numerical simulation has been conducted on the model used by Du et al. [30] and the dimensionless temperature has been plotted along the axial profile (Fig. 3). The porosity of the model has been selected as 0.9. The dimensionless temperature predicted by the numerical model results in a similar trend as reported by Du et al. [30]. The minute differences in the values predicted for non-dimensional temperature can be attributed to different numerical schemes used in this study. Both models can predict that with, $\frac{L}{D} > 140$, $\frac{\partial \theta}{\partial x} = 0$. In other words, the flow becomes fully developed inside the channel when it is empty. However, when the channel is filled with a porous

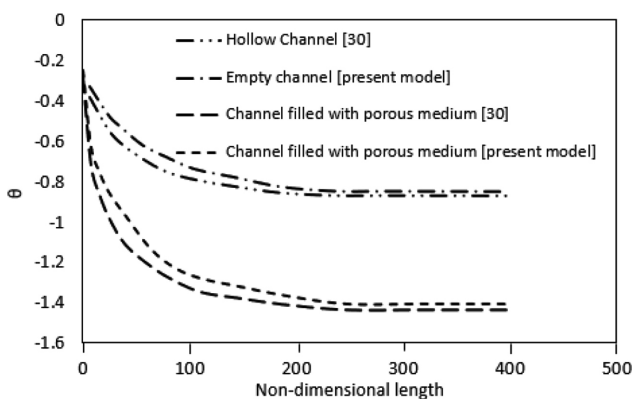


Figure 3. Variation of non-dimensional temperature with non-dimensional length.

medium, a similar phenomenon is observed when $\frac{L}{D} > 190$. This is mainly governed by the presence of a porous matrix inside the channel that redistributes the flow and enhances the length of the fluid entrance region. Comparison of the data in Fig. 3 shows similar trend with a deviation of approximately 3 % between the data predicted by this computational model and that used by Du et al. [30].

RESULTS AND DISCUSSION

Temperature Distribution

Figure 4 shows the variation of non-dimensional temperature as a function of radius of the duct. Numerical simulation predicted a parabolic variation for non-dimensional temperature when studied as function of radius. It can be observed that the non-dimensional temperature for all three types of metal foam studied here 10 PPI, 40 PPI and 60 PPI foam shows minimum value at the center of the duct. It was also observed that 60 PPI foam would result in a minimum non-dimensional temperature of -2.02 whereas that for 10 PPI is -2.81 for the same porosity of $\epsilon = 0.95$. It was also observed that 60 PPI foam would result in a minimum non-dimensional temperature of -2.02 whereas that for 10 PPI is -2.81 for the same porosity of $\epsilon = 0.95$. This is mainly driven by the decrease in the fiber diameter of the foam with increase in the pore density. As the fiber diameter is decreased, the conduction heat transfer increases. Hence the foam with higher pore density is predicted to have higher nondimensional temperature.

Effect of Porosity

Figure 5 illustrates the variation of the Nusselt number as a function of porosity. Numerical simulation predicted that with an increase in porosity there is a marginal decrease in the Nusselt number until $\epsilon = 0.80$ and then begins to drop down sharply. The increase in porosity reduces the fiber diameter of solid phase, thus, increases the conduction heat transport. However, a significant decrease of heat

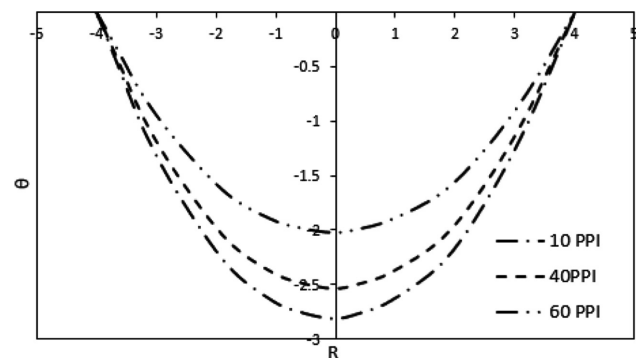


Figure 4. Variation of non-dimensional temperature distribution with radius of the duct.

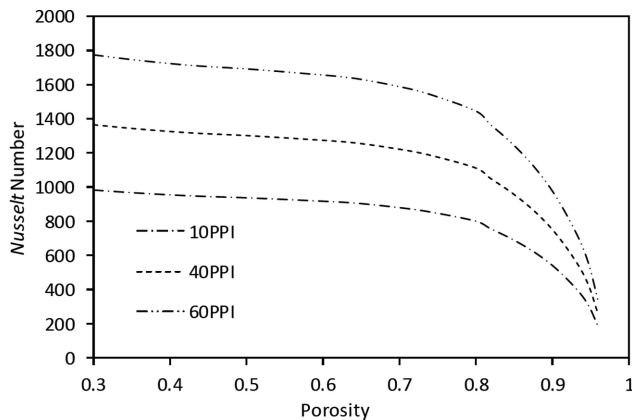


Figure 5. The variation of Nusselt number with porosity for various types of foams.

transfer is caused by the decrease in the fluid velocity due to increased permeability of the solid phase, thus, reducing the convective thermal transport. These two effects lead to a sharp decrease in the Nusselt number with increase in porosity. In this study, porous foam with 10 PPI, 40 PPI and 60 PPI have been observed to exhibit similar variations for Nusselt number when studied with respect to porosity. The data shows a drop of about 81.0 % in Nusselt number when the porosity is increased from 0.3 to 1.0 for all three types of foam studied here. Numerical simulation exhibits that for a given porosity, increasing the pore density results in higher thermal performance (Nusselt number). This is mainly because with an increase in the pore density, fiber diameter decreases and interphase convective heat transfer between the solid and fluid increases.

Effect of Thermal Conductivity Ratio (k_f/k_s)

Figure 6 exhibits the variation of Nusselt number with the ratio of thermal conductivities for fluid to solid. For a given pore density, the variation of Nusselt number becomes significant only when the ratio of thermal conductivities drops below 10^{-4} . The effect is rendered negligible when the ratio increases beyond 0.1. This is primarily because with an increase in the thermal conductivity, the conductive heat transfer becomes more dominating than the convective heat transfer. Consequently, the Nusselt number decreases. Numerical simulation predicted that Nusselt number decreases from 6734 to 2080 when the ratio of thermal conductivity increases from 10^{-5} to 10^{-1} for 10 PPI foam. For porous foam with higher pore densities this reduction in the Nusselt number is from 9649 to 2080 when the ratio of thermal conductivity changes in the same range. It could be seen that there is a drop of 69 % for Nusselt number when the thermal conductivity ratio of fluid to solid increases to 1 from 10^{-5} for 10 PPI foam. However, for 60 PPI foam this decrease is about 79 % for the similar increase in the thermal conductivity ratio.

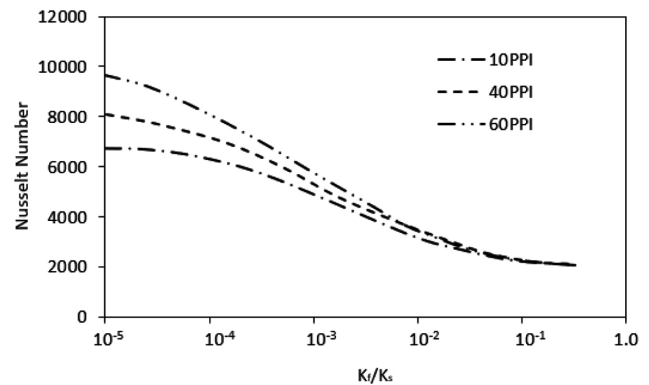


Figure 6. Variation of Nusselt number with the thermal conductivity ratio.

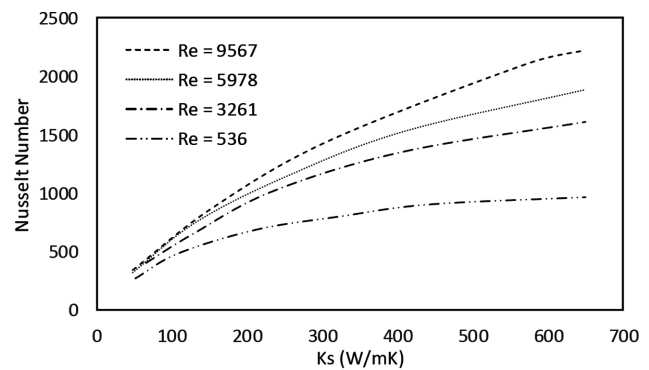


Figure 7. The variation of Nusselt number with solid state thermal conductivity.

Effect of Thermal Conductivity of Porous Medium on Nusselt Number

Figure 7 reflects the variation of the Nusselt number with the thermal conductivity of the foam. With higher Reynold’s number, mass flow rate of the fluid increases, thus increasing the convection heat transfer. Hence, for any given solid-state thermal conductivity, the Nusselt number rises with an increase in Reynold’s number. For any given Reynold’s number, the increase in thermal conductivity of the porous matrix results in higher heat conduction through solid phase. This redistributes the heat to minimize the thermal gradient. This behavior allows the fluid to pass through a larger region of elevated temperature and thus the convection heat transfer increases between the fluid and solid phases. Numerical simulation predicted that for $Re = 536$, Nusselt number increases from 270 to 980 when the thermal conductivity of the solid phase increases from 1 to 600 W/mK. However, for higher Reynold’s number $Re = 9567$, the Nusselt number increases from 410 to 2200 for the same range of solid-state thermal conductivity. From fig.7 it could be seen that for the flow with $Re = 9567$, Nusselt

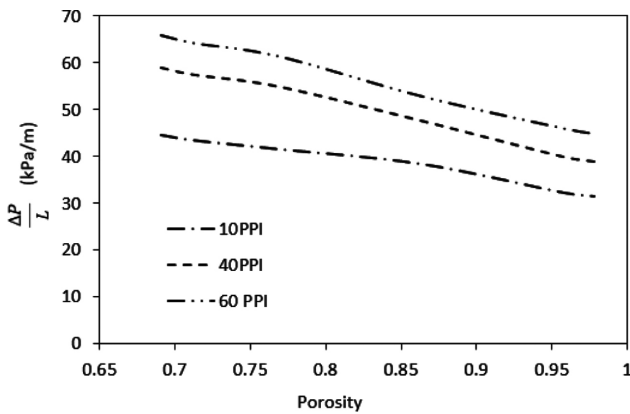


Figure 8. The effect of porosity on pressure drop per unit length for different types of porous foams.

number increases by almost 5.5 times when the solid-state thermal conductivity is increased from 50 to 640. However, for $Re = 536$ this increase is about 2.6 times for the same range of solid-state thermal conductivity variation.

Effect of Porosity on Pressure Drop

Figure 8 exhibits the effect of porosity on the pressure drop per unit length for varying pore densities namely 10 PPI, 40 PPI and 60 PPI. The numerical simulation predicts a drop in the pressure difference per unit length with an increase in porosity. With an increase in the porosity, the volume fraction of solid decreases, thus, to maintain continuity, interstitial fluid velocity decreases and hence, the pressure difference between the inlet and outlet reduces. Similarly, for constant porosity, pressure drop increases with the pore density. The current numerical model calculates a decrease in the pressure drop from 44 KPa/m to 31 KPa/m when the porosity increases from 0.68 to 0.98. For 60 PPI foam, the pressure drop is observed to be from 65 KPa/m to 44 KPa/m for a similar range of porosity. The data shows that with increase in porosity, from 0.65 to 0.98 numerical simulation shows 37 % decrease in pressure drop per unit length when the metal foam was changed from 10 PPI foam to 60 PPI foam.

Effect of Reynolds Number on Pressure Drop

Figure 9 represents the variation of pressure drop per unit length along the tube filled with metal foam as the porous matrix with change in Reynold's number. The numerical prediction exhibits an exponential increase of pressure drop per unit length with an increase in Reynold's number. For 10 PPI metal foam, the numerical simulation predicts an increase in the pressure drop from 4 KPa/m to 61 KPa/m when Reynold's number increases from 1500 to 9300. Similarly, for 60 PPI, the pressure drop per unit length increases from 9.5 KPa to 116 KPa for the similar range of Reynold's number. The data shows that for the duct without porous foam the pressure drop per unit length varies from

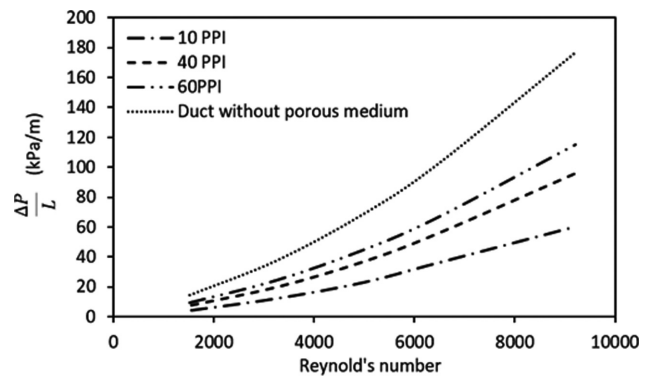


Figure 9. The variation of pressure difference between outlet and inlet, per unit length with Reynold's number.

14.58 kPa/m to 176.58 kPa/m when the Reynolds number is increased from 1500 to 10000. This leads to 2.71 % increase in pressure drop per unit length with every 1 % increase in Reynold's number. However, as the number of pores per inch of the foam increases this increase in pressure drop tends to slow down. Numerical simulation predicted 2.13 % increase in the pressure drop with every 1% rise in Reynold's number for 60 PPI foam studied here. This phenomenon is mainly driven by the increase in the viscous and inertial resistance with increase in Reynold's number. Thus, similar trends were observed for all the three types of porous foams studied here. Hence, it can be said pressure drop per unit length increases with increase in the Reynold's number for the flow.

Variation of Nusselt Number with Reynolds Number

It is interesting to study the relation between Nusselt number and Reynold's number for fluid flow through a pipe filled with a porous medium. Figure 10 exhibits that the Nusselt number increases with an increase in Reynold's number for a given pore density. The increase in Reynold's number results in a higher local heat transfer coefficient. The overall heat transfer coefficient in pipes filled with metal foam is generally comprised of three modes: conductive heat transfer through the metal fibers of the porous matrix, convective heat transfer from the solid to fluid phase and radiative heat transfer due to the hot solid matrix. Depending on the heat flux and temperature of the solid matrix, the contribution of radiative heat transfer can be significant or insignificant. For the current analysis, radiation has been neglected due to the low operating temperature of the solid matrix. Hence, the overall heat transfer depends on the thermal resistances of the solid and fluid. The thermal resistance of the solid is dependent on the porosity, thermal conductivity of the foam and geometrical dimension of the pipe. Whereas that of the fluid depends on the fluid properties and the solid-fluid contact area. The increase of pore density of metal foams increases the conduction area of the solid fibers and the convection heat

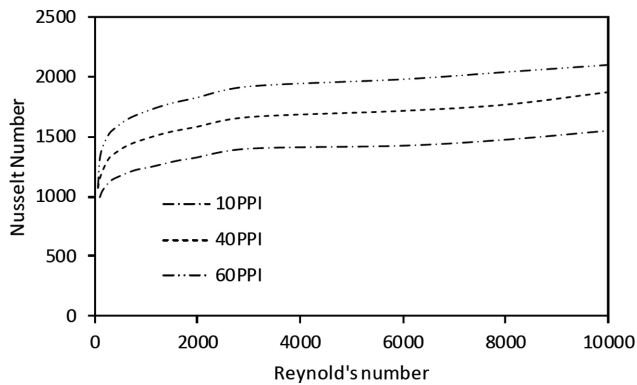


Figure 10. The variation of Nusselt number with change in Reynold's number.

transfer area. This reduces the thermal resistance of both solid and fluid phases and hence increase the overall heat transfer. Additionally, with an increase in Reynold's number fluid mass flow rate increases which further enhances the convective heat transfer. As a result, the Nusselt number increases with the increase of Reynold's number.

Figure 10 also gives insights about the variation of Nusselt number with pore density for a given Reynold's number. The increase in the pore density reduces the pore diameter. For a specific porosity, with the decrease in the pore diameter, the fiber diameter also decreases. This enhances the interfacial surface density and leads to an increase in convective heat transfer from solid to fluid phase. An increase in the Reynolds number comes with an increase in the fluid flow velocity, which increases the thermal transport through the fluid phase. Numerical simulation predicts 56% increase in the Nusselt number when the Reynolds number is increased from 100 to 10000 for 10 PPI foam. For 60 PPI foam this increase is 94.5 % for the same range of Reynolds number. Hence with higher pore density, higher heat transfer is achieved for any given value of Reynold's number as illustrated in Fig. 10.

CONCLUSION

Conjugate heat transfer has been studied in a pipe filled with porous foam. Following conclusions were drawn using the computational model:

- a. The data reflects that for a specific porosity use of metal foam with higher pore density results in higher Nusselt number. The numerical model predicted 83.4 % increase in Nusselt number when the pore density is increased from 10 PPI to 60 PPI for $\epsilon = 0.60$. However, the increase in the Nusselt number with increase in pore density is not so significant beyond $\epsilon = 0.86$. This is majorly attributed to the decrease in the fiber diameter with increase in pore density. This decrease in the fiber diameter results in more interfacial heat transfer between the solid and fluid phase.

- b. Numerical simulation shows that with an increase in the ratio of thermal conductivity of the fluid to solid from 10^{-5} to 1.0 there is a sharp decrease ($\sim 74.4\%$) in Nusselt number for 60 PPI foam. However, this decrease is much slower ($\sim 61.2\%$) for 10 PPI foam for the same range of thermal conductivity ratio.
- c. It was observed that with an increase in porosity from 0.65 to 0.98 numerical simulation shows 37% decrease in pressure drop per unit length when the metal foam was changed from 10 PPI foam to 60 PPI foam.
- d. The data shows that even though using metal foams with low porosity and high pore density results in higher heat transfer performance, yet they come with a significant pressure drop. Numerical simulation predicted 2.13% increase in the pressure drop per unit length with every 1% rise in Reynold's number for 60 PPI foam.
- e. It was observed that for flows with Reynold's number < 10000 , increasing the pore density of 10 PPI to 60 PPI results in 38.7 % gain in Nusselt number.

Based on the constraints of pumping power, this study recommends the use of low porosity porous material with low pore densities.

NOMENCLATURE

a_{sf}	Specific surface area
h_{sf}	Interfacial heat transfer coefficient
D	Inner diameter of pipe
k_s	Thermal conductivity of the solid
k_f	Thermal conductivity of the fluid
k_{se}	Effective thermal conductivity of the solid
k_{fe}	Effective thermal conductivity of the fluid
L	Length of the pipe
P	Pressure
q	Heat flux
r_i	Inner radius of the pipe
r_o	Outer radius of the pipe
t	Thickness of the pipe
T_s	Solid-phase temperature
T_w	Wall temperature
T_f	Fluid-phase temperature
u	Fluid axial velocity
v	Radial fluid velocity
Re	Reynold's number
Greek symbols	
μ	Dynamic viscosity of the fluid
ϵ	Porosity
θ	Non dimensional temperature, $\frac{T - T_w}{q \frac{R}{k_{se}}}$
$\Delta P/L$	Pressure difference between outlet and inlet measured per unit length

AUTHORSHIP CONTRIBUTIONS

Authors equally contributed to this work.

DATA AVAILABILITY STATEMENT

The authors confirm that the data that supports the findings of this study are available within the article. Raw data that support the finding of this study are available from the corresponding author, upon reasonable request.

CONFLICT OF INTEREST

The author declared no potential conflicts of interest with respect to the research, authorship, and/or publication of this article.

ETHICS

There are no ethical issues with the publication of this manuscript.

REFERENCES

- [1] Vafai K, Tien CL, Boundary and inertia effects of flow and heat transfer in porous media, *Int. J. Heat Mass Transf* 1981;24:195–203. [\[CrossRef\]](#)
- [2] Whitaker S. Flow in Porous Media I: A Theoretical Deviation of Darcy's Law, *Trans. In Porous Media*, 1986;03:25–30. [\[CrossRef\]](#)
- [3] Fand RM, Steinberger TE, Cheng P. Natural convection heat transfer from a horizontal cylinder embedded in porous medium. *Int J Heat Mass Transf* 1986;29:119–133. [\[CrossRef\]](#)
- [4] Calimadi VV. Transport phenomena in high porosity fibrous metal foams. Doctoral Thesis. University of Colorado, 1988.
- [5] Suces J. Analytical solution for unsteady heat transfer in a pipe. *J Heat Transf* 1988;110:850–854.
- [6] Lin TF, Kuo JC. Transient conjugated heat transfer in fully developed laminar pipe flows. *Int J Heat Mass Transf* 1988;31:1093–1102. [\[CrossRef\]](#)
- [7] Olek S, Elias E, Wacholadr E, Kaizweman S. Unsteady conjugated heat transfer in laminar pipe flow. *Int J Heat Mass Transf* 1995;34:1443–1450. [\[CrossRef\]](#)
- [8] Kim SJ, Kim D, Lee DY. On the local thermal equilibrium in microchannel heat sinks. *Int J Heat Mass Transf* 2000;43:1735–1748. [\[CrossRef\]](#)
- [9] Boomsma K, Paulikakos D. On the effective thermal conductivity of three-dimensional structured fluid-saturated metal foam. *Int J Heat Mass Transf* 2001;44:827–836. [\[CrossRef\]](#)
- [10] Bhattacharya A, Calmidi VV, Mahajan RL. Thermophysical properties of high porosity metal foams. *Int J Heat Mass Transf* 2002;45:1017–1031. [\[CrossRef\]](#)
- [11] Nazar R, Amin D, Filip I. The Brinkman model for the mixed convection boundary layer flow past a horizontal circular cylinder in a porous medium. *Int J Heat Mass Transf* 2003;46:3167–3178. [\[CrossRef\]](#)
- [12] Zhao CY, Lu TJ, Hodson HP. Natural convection in metal foams with open cells. *Int J Heat Mass Transf* 2005;48:2452–2463. [\[CrossRef\]](#)
- [13] Lu W, Zhao CY, Tassou SA. Thermal analysis on metal-foam filled heat exchangers. Part I: Metal-foam filled pipes. *Int J Heat Mass Transf* 2006;49:2751–2761. [\[CrossRef\]](#)
- [14] Zhao CY, Lu W, Tassou SA. Thermal analysis on metal-foam filled heat exchangers. Part II: Tube heat exchangers. *Int J Heat Mass Transf* 2006;49:2762–2770. [\[CrossRef\]](#)
- [15] Mahjoob S, Vafai K. A synthesis of fluid and thermal transport models for metal foam heat exchangers. *Int J Heat Mass Transf* 2008;51:3701–3711. [\[CrossRef\]](#)
- [16] DeGroot CT, Straatman AG, Betchen JL. Modeling forced convection in finned metal foam heat sinks. *ASME J Electron Pack* 2009;131:021001–021010. [\[CrossRef\]](#)
- [17] Dhukan N, Bagci O, Ozdemir M, Kavurmacioglu L. Experimental fully developed thermal convection for non-darcy water flow in metal foam. *J Therm Eng* 2016;2:677–682. [\[CrossRef\]](#)
- [18] Arbak A, Bagci O, Dukhan N. Flow regimes in commercial metal foam having 10 pores per inch. *J Therm Eng* 2016;2:1023–1028. [\[CrossRef\]](#)
- [19] Banerjee A, Saveliev AV. High temperature heat extraction from counterflow porous burner. *Int J Heat Mass Transf* 2018;127:436–443. [\[CrossRef\]](#)
- [20] Banerjee A, Saveliev AV, Effect of heat extraction on flame position in counterflow porous burner. *ASTFE Digital Lib*, 2019. [\[CrossRef\]](#)
- [21] Banerjee A, Kundu P, Gnatenko V, Zelepouga S, Wagner J, Chudnovsky Y, et al. NOx minimization in staged combustion using rich premixed flame in porous media. *Comb Sci Technol* 2019;1–17. [\[CrossRef\]](#)
- [22] Banerjee A, High temperature heat recirculation from heat recirculating porous burner, Doctoral Thesis. North Carolina State University, 2019.
- [23] Mosayebidorcheh SS, Vatani M, Mosayebidorcheh T, Hatami M, Ganji DD. Differential transformation method for analysis of nonlinear flow and mass transfer through a channel filled with a porous medium. *J Therm Eng* 2020;6:24–40. [\[CrossRef\]](#)
- [24] Banerjee A, Saveliev AV. Emission characteristics of heat recirculating porous burner with high temperature energy extraction. *Front Chem* 2020;8–20. [\[CrossRef\]](#)

-
- [25] Hotte F, Haupt MC. Transient 3D conjugate heat transfer simulation of a rectangular GOX–GCH₄ rocket combustion chamber and validation. *Aero Sci Technol* 2020;105:1043–1060. [\[CrossRef\]](#)
- [26] Ferguson JC, Sobhani S and Ihme M, Transient 3D conjugate heat transfer simulation of a rectangular GOX–GCH₄ rocket combustion chamber and validation, *Proc. Comb Inst*, 2020, In press.
- [27] Banerjee A, Paul D, Develoments and applications of porous medium combustion: A recent review, *Energy*, 2021 (In-press). [\[CrossRef\]](#)
- [28] Banerjee A, Roy S, Mukherjee P, Saha UK, Unsteady flow analysis around an elliptic-bladed Savonius-style wind turbine, *Gas Turbine India Conf.*, 2014, 49644, V001T05A001. [\[CrossRef\]](#)
- [29] Banerjee A. Performance and flow analysis of an elliptic bladed Savonius-style wind turbine. *J Renew Sustain Energy* 2019;11:003–3307. [\[CrossRef\]](#)
- [30] Du YP, Qu ZG, Zhao CY, Tao WQ. Numerical study of conjugated heat transfer in metal foam filled double-pipe. *Int J Heat Mass Transf* 2010;53:4899–4907. [\[CrossRef\]](#)